JOURNAL OF GEOPHYSICAL RESEARCH, VOL. 108, NO. D19, 4613, doi:10.1029/2002JD003025, 2003

Correction published 29 November 2003

Multiscale interactions between surface shear stress and velocity in turbulent boundary layers

V. Venugopal, F. Porté-Agel, E. Foufoula-Georgiou, and M. Carper
St. Anthony Falls Laboratory, University of Minnesota, Minneapolis, Minnesota, USA

Received 8 October 2002; revised 20 May 2003; accepted 12 June 2003; published 11 October 2003.

[1] Understanding and quantifying the multiscale interactions between surface shear stress and velocity in the boundary layer is essential to improving boundary condition parameterizations used in numerical models of turbulent boundary layers. In this study, high-frequency measurements obtained in a wind tunnel are used to identify dominant scales of interaction (quantified in terms of scale-dependent linear correlation) between wind velocity and shear stress via wavelet cross-correlation analysis. Three ranges of scales of interaction are identified: (1) in the inertial subrange the correlation is negligible; (2) in the energy production range the correlation follows a logarithmic law and exhibits scale invariance under normalization of scale with distance to the surface, z; and (3) for scales larger than the boundary layer height, δ, the correlation reaches a plateau value which is a function of z/δ. Our results allow us to estimate the linear correlation between shear stress and wind velocity at multiple scales and assess the reliability of typical boundary condition formulations in numerical models (for instance, large-eddy simulation) that compute shear stress (or its fluctuations) as a linear function of wind velocity at the first vertical grid point. *INDEX TERMS:* 3307 Meteorology and Atmospheric Dynamics: Boundary layer processes; 3322 Meteorology and Atmospheric Dynamics: Land/atmosphere interactions; 3337 Meteorology and Atmospheric Dynamics: Numerical modeling and data assimilation; *KEYWORDS:* wavelets, shear stress, boundary layers

Citation: Venugopal, V., F. Porté-Agel, E. Foufoula-Georgiou, and M. Carper, Multiscale interactions between surface shear stress and velocity in turbulent boundary layers, *J. Geophys. Res.*, *108*(D19), 4613, doi:10.1029/2002JD003025, 2003.

1. Introduction

[2] Flow properties, such as velocity and surface shear stress, in turbulent boundary layers (e.g., the atmospheric boundary layer (ABL)) exhibit considerable variability over a broad range of spatial and temporal scales. Understanding the multiscale interactions between these flow properties is essential to improving parameterizations used in high-resolution numerical models of turbulent transport. For instance, an important parameterization in large-eddy simulation (LES) is the surface boundary condition which relates the surface shear stress to the "resolved" velocity. Typical boundary condition formulations consist of using similarity theory to compute the surface shear stress as a linear function of the horizontal velocity (spatially filtered with a filter of size equal to or slightly larger than the grid size). However, similarity theory is valid only for mean quantities and over homogeneous surfaces. This approach is therefore questionable for general unsteady conditions and over heterogeneous natural surfaces (in the ABL). Given the importance of the boundary condition on the dynamics of the flow near the surface, obtaining physically more realistic boundary condition formulations has been recognized as one of the most urgent challenges that needs to be met to make LES a more reliable tool in simulations of high-Reynolds-number boundary layers in both engineering and environmental applications [*Piomelli et al.*, 1999; *Piomelli and Balaras*, 2002]. In order to achieve this goal, we need a better understanding of the relation between the surface shear stress and the velocity at different scales, particularly at the grid/filter scale in a simulation. To this end, wavelets [e.g., see *Mallat*, 1989a, 1989b; *Daubechies*, 1992] provide a convenient and powerful framework to probe into the scales of complex interactions between these two processes.

[3] Over the last decade, starting with the works of *Meneveau* [1991] and *Farge* [1992], wavelet transforms have been successfully applied to study atmospheric turbulence. The studies have ranged from identifying coherent structures from time series of velocity and temperature in the atmospheric boundary layer [e.g., *Hagelberg and Gamage*, 1994; *Howell and Mahrt*, 1994; *Brunet and Collineau*, 1994], to investigating intermittency [*Katul et al.*, 1994], to exploring energy cascading in the dynamic sublayer [*Katul and Chu*, 1998], to studying the effect of topography on the scales of response of a simulated convective boundary layer [*Roy and Avissar*, 2000]. Correlation measures in the wavelet domain were used by *Meneveau and Lund* [1994] to show that propagation of kinetic energy from a particular scale to smaller scales can be characterized by a peak in the correlation coefficient between local kinetic energies at different scales. Along similar lines, *Arnéodo et*

0148-0227/03/2002JD003025$09.00

al. [1998] used space-scale correlations obtained from wavelet transforms of turbulent velocity signals to identify what kinds of multiplicative cascades (correlated weights or not) can be used to statistically model turbulence.

[4] The purpose of this work is to quantify the multiscale interactions between surface shear stress and velocity over a homogeneous surface and discuss the implications of our results toward characterizing the surface boundary condition in high-resolution models. The spatial and temporal information about the flow properties in a boundary layer needed to study the aforementioned multiscale interactions cannot be obtained in the field, even with state-of-the-art measurement techniques. On the other hand, a wind tunnel offers an optimal setting for controlled experiments, wherein simultaneous high-frequency measurements of the surface shear stress and the velocity field can be obtained using special hot wire and hot film sensors mounted on the surface of the tunnel [see *Chew et al.*, 1998; *Marusic et al.*, 2001]. Such data have been used in our analysis and are described in section 2.

[5] In section 3 a theoretical background on wavelet-based analysis techniques is presented. The results of applying these methodologies to decompose the cross correlation between shear stress and velocity series at multiple scales are presented in section 4. The implications of our findings in improving surface boundary condition parameterization are elaborated in section 5. Finally, section 6 summarizes our findings and discusses future research.

2. Data Description

[6] The data analyzed in this work were collected by I. Marusic et al. at the University of Minnesota. The reader is referred to *Marusic et al.* [2001] for a detailed description of the data collection procedures (sensor calibration, correction, etc.). Only a brief description of the measurement setup is provided here. The working section of the wind tunnel is 1.2 m wide, 4.7 m long, and nominally 0.3 m high. Measurements were made at a location 3.2 m downstream of a trip wire, where the boundary layer thickness (hereinafter referred to as δ) is 64 mm. The Reynolds number based on momentum thickness $R_\theta = U_1\,\theta/\nu = 3500$, where θ is momentum thickness and $U_1 = 8.9$ m s^{-1} is the free stream velocity. This corresponds to a Karman number, $Re_\tau = U_\tau\,\delta/\nu = 350$, where U_τ ($= \sqrt{-\tau_w/\rho}$; τ_w is the mean wall shear stress, and ρ is the density of the fluid) is the shear velocity (m s^{-1}) and ν is the kinematic viscosity (m^2 s^{-1}). In all, the experimental setup contains nine wall shear stress sensors (TSI hot film) and three velocity sensors (x wire probes). In this study we used data from one wall-mounted shear stress sensor and one velocity sensor located immediately above the shear sensor. In addition, in order to study how the interaction between shear stress and velocity changes with height, the velocity sensor was positioned at six different heights (measured from the surface), $z \approx 4.7$, 5.9, 7.5, 9.4, 11.9, and 15×10^{-3} m. The equivalent wall-normal positions are $z^+ = zU_\tau/\nu = 98$, 123, 155, 196, 247, and 311, respectively. Velocity and shear stress measurements were made at a frequency of 10 kHz over a time period of 105 s. Figure 1 shows a small sample of the measurements taken when the velocity sensor was positioned at a height of 4.7 mm.

[7] The first step in studying the correlation between shear stress and velocity is to perform a standard cross-correlation analysis between u and τ for different positions of the velocity sensor (see Figure 2a). (A standard two-point linear correlation between u and τ is computed, i.e., $C_{u,\tau}(\Delta t) = E[(u(t) - \overline{u}), (\tau(t + \Delta t) - \overline{\tau})]/(\sigma_u\sigma_\tau)$, where $\overline{u}$ and $\overline{\tau}$ represent the mean of u and τ, respectively.) As expected, the maximum correlation decreases with increasing sensor height. Furthermore, the lag to maximum correlation increases with sensor height in a manner consistent with the hypothesis of *Piomelli et al.* [1989], which asserts that eddies develop as structures inclined at an angle of $\sim 12^\circ - 15^\circ$ to the surface (see Figure 2b).

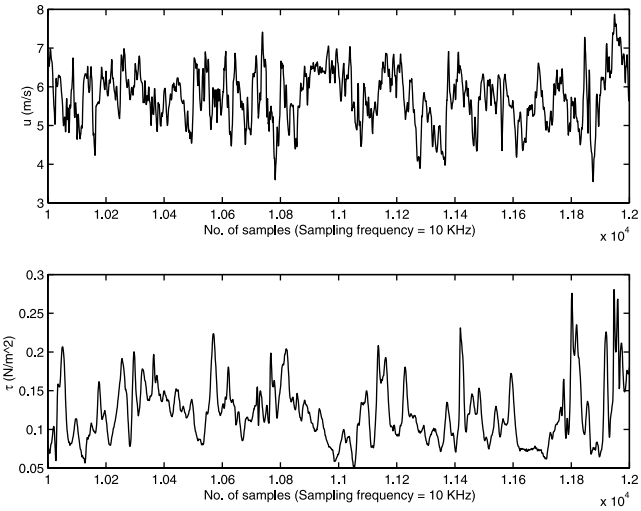

Figure 1. (top) Horizontal velocity, u (m s^{-1}), measured at $z = 4.7$ mm and (bottom) shear stress, τ (N m^{-2}). The overall record length is 105 s at a frequency of 10 kHz ($\sim 10^6$ points). A sample of size 2000 points is shown in the above plots.

[8] It is important to note here that the correlation between two multiscale processes (characterized by the presence of energy over a broad range of scales, as is the case with shear stress and velocity) can be decomposed into correlations at multiple scales. In other words, if one were able to represent two multiscale processes as a combination of "functions" at different scales, then a simple two-point linear correlation between the components (at different scales) would quantify the contribution of each scale to the overall correlation and would thus help one understand the scale-to-scale interaction between the two processes. To this end, wavelet transforms, which have seen significant theoretical developments and applications in the past decade, provide a convenient framework in which to study the contribution of correlations from multiple scales. Section 3 defines the relevant quantities to aid the reader with the terminology used in our multiscale analysis.

3. Wavelet-Based Analysis: Theoretical Background

[9] The wavelet transform of a function $f(t)$ with finite energy is defined as the integral transform with a family of functions:

$$\psi^{a,b}(t) = \frac{1}{\sqrt{a}}\psi\left(\frac{t-b}{a}\right); a > 0; b \in \mathcal{R},$$

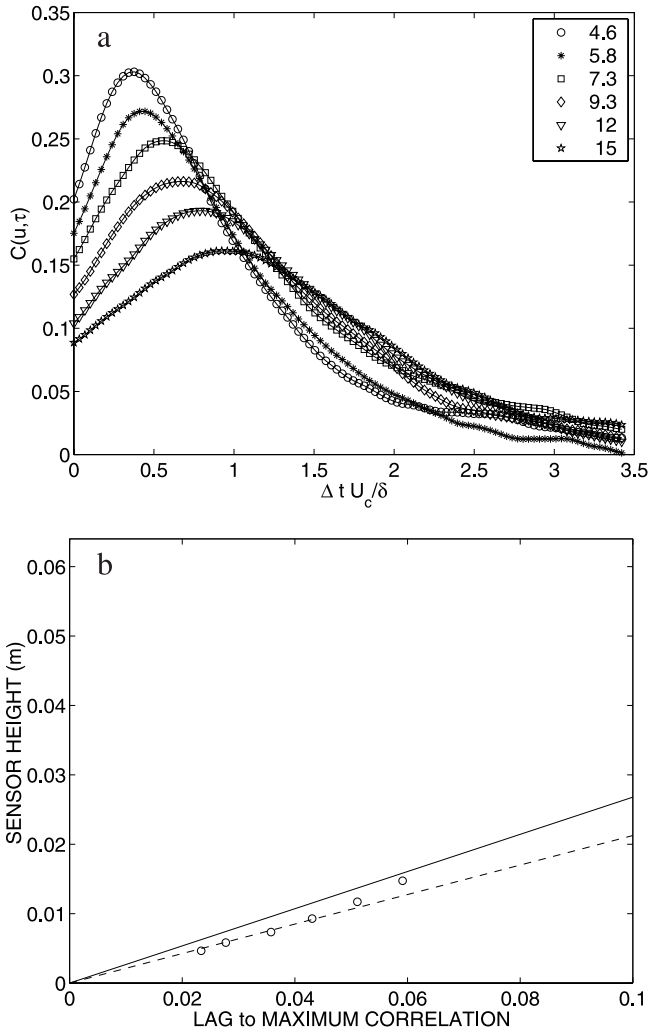

Figure 2. (a) Two-point linear correlation between velocity (u) and shear stress (τ) for different sensor heights (legend shows sensor height in mm). The maximum correlation, as anticipated, decreases with increasing sensor height. (b) Lags to maximum correlation within the lines of 12° (dashed line) and 15° (solid line), consistent with the hypothesis of *Piomelli et al.* [1989] that flow structures near the surface are inclined at an angle of 12°–15° with respect to the surface. $U_c = 0.8U_1$, where $U_1 = 8.9$ m s^{-1} is the free stream velocity.

all generated by translation (by b) and dilation or contraction (by a factor of a) from a single function ψ, called the "mother wavelet." A necessary condition for a function to be admissible as a wavelet is one of zero mean, to ensure that the transform is invertible [e.g., see *Daubechies*, 1992]. Thus the continuous wavelet transform (CWT) of a function f is defined as

$$W_f(a,b) = |a|^{-\frac{1}{2}} \int f(t)\psi\left(\frac{t-b}{a}\right)dt, \tag{1}$$

where a is the scale parameter and b is the location parameter. The factor $1/\sqrt{a}$ is a normalization constant chosen to ensure that the $\mathcal{L}^2$ norm is preserved. For some applications the normalization factor of $1/a$ is used, which preserves the $\mathcal{L}^1$ norm. Several choices of a wavelet can be made; some popular wavelets include the second derivative of a Gaussian (commonly called Mexican Hat), the Morlet, the Haar, and the Daubechies wavelets.

[10] Once the function is transformed into the wavelet domain, a suite of measures can be defined to quantify localized scale-dependent properties of the function. For example, two such measures are the scalogram, defined as $|W_f(a, b)|^2$, and the wavelet variance, or wavelet spectrum (in essence, this is similar to the Fourier spectrum), defined as

$$\mathrm{WV}_f(a) = \int_{-\infty}^{\infty} \left|W_f(a,b)\right|^2 db. \tag{2}$$

[11] For two signals or functions containing energies at multiple scales, cross-correlation analysis in the wavelet space often offers valuable insight. For example, the wavelet covariance of two functions f and g is defined as

$$\mathrm{WCOV}_{fg}(a) = \int_{-\infty}^{\infty} W_f(a,b)W_g(a,b)db \tag{3}$$

and measures the "correlation" of the functions f and g as far as the "entities" of length scale a are concerned. In other words, the correlation of the two functions is decomposed across scales.

[12] The covariance of two functions can, in turn, be related to the wavelet covariance by the following relation:

$$\mathrm{COV}(f,g) = \frac{1}{C_\psi} \int da \int W_f(a,b)W_g(a,b)db,$$

where $C_\psi = 2\pi \int |\omega|^{-1}|\hat{\psi}(\omega)|^2 d\omega < \infty$ is the so-called "admissibility constant," a localizing property of the decomposing wavelet [see *Daubechies*, 1992].

[13] For processes that interact dynamically across scales, one anticipates that the strongest cross correlations might not always exist at concurrent times over all ranges of scales. This motivates the introduction of time lag Δt in the above definition of wavelet covariance, leading to what might be referred to as the wavelet cross covariance, defined as

$$\mathrm{WCCOV}_{fg}(a,\Delta t) = \int_{-\infty}^{\infty} W_f(a,b)W_g(a,b+\Delta t)db. \tag{4}$$

With appropriate normalization by the variance of each of the functions in the integral, one can obtain the wavelet cross correlation. It is important to mention here the value of using a localized representation such as wavelet transform, as opposed to a Fourier decomposition, which is global in nature. While equation (3) is similar to the product of Fourier transforms, equation (4) cannot be obtained using a classical Fourier transform (because of the lag Δt) unless one uses a windowed Fourier transform, which, in any case, is a special case of wavelet transforms. The wavelet used for our analysis is the second derivative of a Gaussian, popularly known as

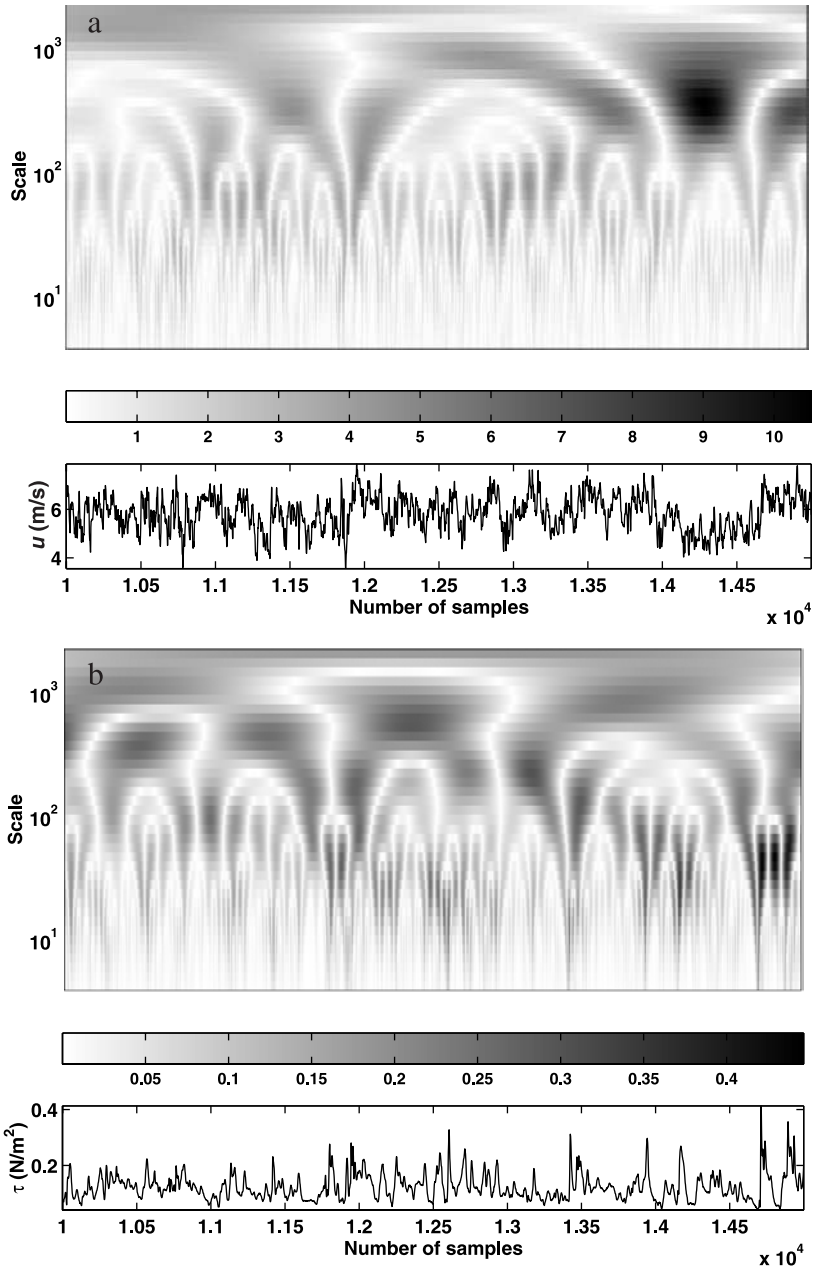

Figure 3. Timescale plots, obtained by wavelet analysis, of (a) observed horizontal velocity at height $z = 4.7$ mm and (b) observed shear stress. The scale shown on the y axis is in number of points.

the "Mexican Hat Wavelet," which has a functional form $\psi(x) = \pi^{-1/4}\ (1 - x^2)\ e^{-x^2/2}$.

4. Results and Discussion

[14] In all, 500,000 sampled values of velocity and shear stress time series were included in the analysis. The scales analyzed ranged from 2 to 8000 points (the equivalent timescales range from 2×10^{-4} to 0.8 s, given that the sampling frequency is 10 kHz).

[15] Figure 3 shows a part of the timescale plot (the square of the wavelet coefficients or, equivalently, the energy at that time and frequency/scale, with associated uncertainties governed by the Heisenberg uncertainty principle) for velocity (Figure 3a) and shear stress (Figure 3b). The branching of energy from larger to smaller scales, for both variables, is evident from these plots. To aid the reader in visualizing the decompositions across scales, Figure 4 displays the transects through the timescale plots of Figure 3 at two different scales.

[16] If one were to sum up the squares of wavelet coefficients at each scale (level), that would give the equivalent of contribution of energy from each scale (an average levelwise energy) to the overall energy. In other words, the sum of the squares of the amplitudes of the decomposed signals, such as those shown in Figure 4, results in a spectrum of energy (called the wavelet spectrum). Figure 5a shows the wavelet spectrum of velocity for different vertical positions of the sensor. Several well-known facts can be noted in Figure 5a. In particular, the

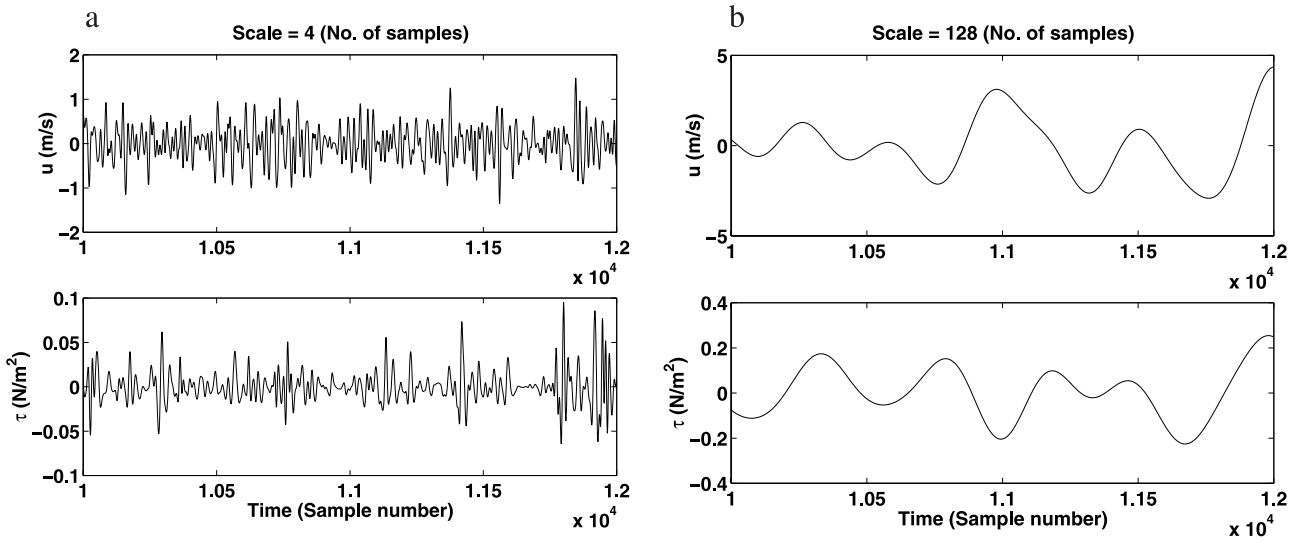

Figure 4. Transects of the timescale plots of Figure 3 at scales corresponding to (a) 4 points and (b) 128 points. The corresponding timescales are 4×10^{-4} and 128×10^{-4} s, respectively. The top panels represent the wavelet decomposition, i.e., the wavelet coefficients of horizontal velocity ($z = 4.7$ mm) at the two chosen scales, and the bottom panels represent the decomposition of shear stress.

existence of three ranges of scaling is evident: (1) inertial subrange, characterized by a spectral slope of $-5/3$; (2) energy production subrange, showing a -1 spectral slope; and (3) scales larger than the integral length scale (on the order of the boundary layer height), characterized by a flat region (i.e., no change in contribution to the total energy with increase in scale). As expected, and as shown in several previous studies [e.g., see *Perry et al.*, 1986; *Porté-Agel et al.*, 2000], under appropriate normalization of both the energy (by zU_τ^2) and the wave number, k (by z), the spectra obtained from each sensor collapse onto each other in the production and the inertial subranges, with the transition from the inertial to production subrange occurring at $(kz,\ E(a)/zU_\tau^2) \approx (1,1)$. Figure 5b shows the wavelet spectrum of shear stress. While the evidence is clear that its "energy" (spectral density) is distributed over a wide range of scales, there is no indication suggesting the existence of scaling ranges similar to velocity.

[17] Similar to the quantification of the contribution of energy at each scale to the overall energy, one can also evaluate the contribution of correlation at each scale to the overall correlation. Denoted as $C_{u,\tau}^{\mathrm{CWT}}(a,\ \Delta t)$, this is equivalent to computing the two-point cross correlation between pairs of transects at different timescales (e.g., the time series in Figure 4) and time lags (see equation (4)). In other words, $C_{u,\tau}^{CWT}\ (a,\ \Delta t)$ is the same as the wavelet cross covariance (equation (4)) normalized by the product of the wavelet variance of u and τ at each scale. Thus this correlation is a function of two variables, timescale and time lag. The cross correlation between the scale-decomposed velocity (at $z = 4.7$ mm) and shear stress is shown in Figure 6. (It is noted that the timescale is normalized to be dimensionless in Figure 6. This is done by a combination of two factors: (1) a length scale that corresponds to the distance between the velocity and shear stress sensors, z, and (2) a velocity scale, $\overline{u}$, which corresponds to the average velocity at height z. Such a normalization (whose importance is discussed later in this section) results in a quantity equivalent to kz, as obtained via application of Taylor's hypothesis, shown in the velocity spectra of Figure 5a. We use kz for the rest of the discussion.)

[18] Several observations can be made from this plot. The first relates to the existence of ranges of scales, within which the contribution of correlation to the overall correlation is markedly different. Contributionwise, three distinct regions are identified: (1) negligible correlation at "small" scales; (2) significant correlation increasing with scale at "intermediate" scales; and (3) significant and constant correlation at "large" scales. To reduce this surface plot into a line plot, which would enable one to understand better the significance of these three ranges of scales, and with the explicit understanding that the behavior at any lag, i.e., a cross section of the surface at any lag, is qualitatively the same, we chose to study the dependence of maximum correlation with scale (see the bold solid line in Figure 6).

[19] The analysis was repeated for all positions of the sensor, and the maximum correlation (MC) is plotted as a function of scale (Figure 7). (Correlation, by definition, is dimensionless; hence there is no need to normalize it, as done for energy in the velocity spectral plots.) This results in the maximum correlation curves collapsing onto each other. As in the case of velocity spectral collapse (Figure 5a), there are two ranges of scales in which the MC curves collapse; these ranges correspond to the inertial and production subrange, while beyond the boundary layer height (integral length scale), there is no apparent collapse. The collapse of the MC curves suggests an invariance concerning the size of the eddy to the height of the sensor, i.e.,

$$\mathrm{MC}_{u,\tau}^{\mathrm{CWT}}(k_1, z_1) = \mathrm{MC}_{u,\tau}^{\mathrm{CWT}}(k_2, z_2),\ \text{if}\ k_1 z_1 = k_2 z_2 = kz \gtrsim z/\delta,$$

where $\mathrm{MC}_{u,\tau}^{\mathrm{CWT}}\ (k,\ z)$ denotes the maximum correlation at scale k between u (at height z) and τ, as obtained from a CWT analysis.

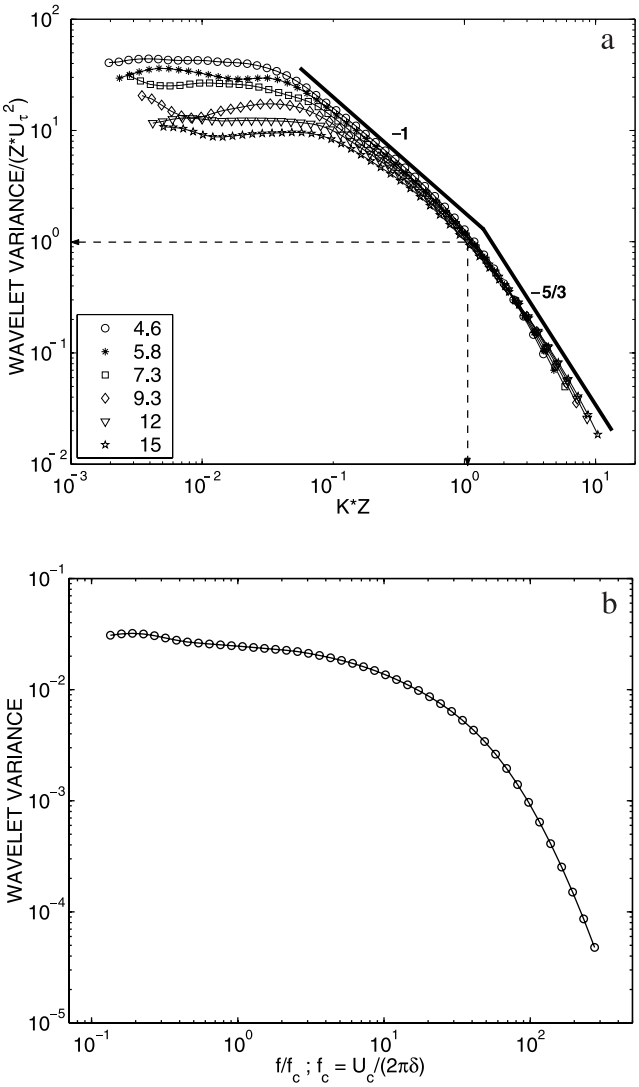

Figure 5. (a) Wavelet spectrum of u. (b) Wavelet spectrum of τ. The production subrange (-1 slope) and the inertial subrange ($-5/3$ slope) can be clearly identified. See the text for additional details concerning the collapse of spectral curves and the associated normalization. $U_c = 0.8U_1$, where $U_1 = 8.9$ m s^{-1} is the free stream velocity, and f is the frequency or inverse of the wave number (k) at which the signal has been decomposed.

[20] In other words, the correlation between shear stress and velocity associated with eddies of size Δ ($\sim 1/k_1$) measured at a height z_1 is identical to that from eddies of size $3\Delta(\sim 1/k_2)$ measured at a height $3z_1$ (z_2). This scale invariance breaks down at scales larger than the boundary layer height. This is to be expected since the largest possible eddy scales are constrained by the thickness of the boundary layer.

[21] In the inertial subrange ($kz \gtrsim 1$) the contribution to correlation from each scale is negligible. This is (intuitively) consistent with the fact that eddies are smaller than the height of the sensor, and thus the eddies that pass through the velocity sensor will not be detected by the shear sensor, leading to a negligible correlation. For $kz \lesssim 1$ (production subrange), i.e., the eddy size is larger than the sensor height, resulting in eddies being detected simultaneously by both the shear and velocity sensors, one would expect an increase in correlation, and this is evident in Figure 7. Furthermore, the plot of Figure 7 suggests that in the production subrange the increase follows a logarithmic law, with a slope of $-1/2$. Beyond the boundary layer height ($kz \lesssim z/\delta$) the relative effect of larger structures in contributing to correlation is dampened, as evidenced by the plateau in the MC curves.

[22] The fact that the MC curves for all sensor heights show a value of zero in the inertial subrange and a constant value (depending on the boundary layer height) in the range of scales corresponding to boundary layer height and beyond (integral-length scale), with a log law in the production subrange, suggests a possible universality in the dependence of correlation on scale, as described by the following relation:

$$\mathrm{MC}_{u,\tau}^{\mathrm{CWT}}(k,z) \approx \begin{cases} 0 & kz \gtrsim 1 \\ \xi \log(kz) & z/\delta \lesssim k \gtrsim 1 \\ \xi \log(z/\delta) & kz \lesssim z/\delta \end{cases} \quad (5)$$

The parameter ξ in the log law was estimated to be $-1/2$ for our data and (experimental) conditions. It is speculated that while the behavior (collapse of MC curves in the production subrange) is expected to be universal for any turbulent boundary layer, the slope ξ is a function of several parameters of the flow conditions (e.g., Reynolds number, buoyancy) and surface properties (e.g., land surface heterogeneity in the ABL). For instance, with increasing Reynolds number, we expect to observe a decrease in the slope of the log law ξ so as to be able to accommodate a wider range of eddy scales. Furthermore, the dependence of the correlation maximum on kz is expected to be independent of surface roughness z_o as long as z is in the surface layer and $z \gg z_o$, which corresponds to the region of the flow where similarity theory holds (log layer). This is supported by the fact that the inertial and production subranges are found in any wall-bounded turbulent flow, independent of Reynolds number and surface roughness (including the ABL). The results are only expected to depart from that behavior very close to the surface, inside the roughness sublayer (z close to z_o), which, in most cases, has little practical significance from a modeling point of view.

5. Implications for Boundary Condition Formulations

[23] Before we discuss the importance of our results in understanding the performance and limitations of the surface boundary condition for LES of high-Reynolds-number boundary layers, we briefly review the two most typical boundary condition formulations:

[24] 1. A common formulation consists of computing the streamwise component of the surface shear stress (τ) as proportional to the filtered streamwise velocity ($\tilde{u}$) at the first vertical grid point [e.g., see *Schumann*, 1975; *Porté-Agel et al.*, 2000; *Piomelli and Balaras*, 2002]. Mathematically, this can be expressed as

$$\tau = \frac{\langle \tau \rangle}{\langle \tilde{u} \rangle} \tilde{u}, \quad (6)$$

where angle brackets denote ensemble averaging and the tilde denotes spatial filtering (using a low-pass filter of a

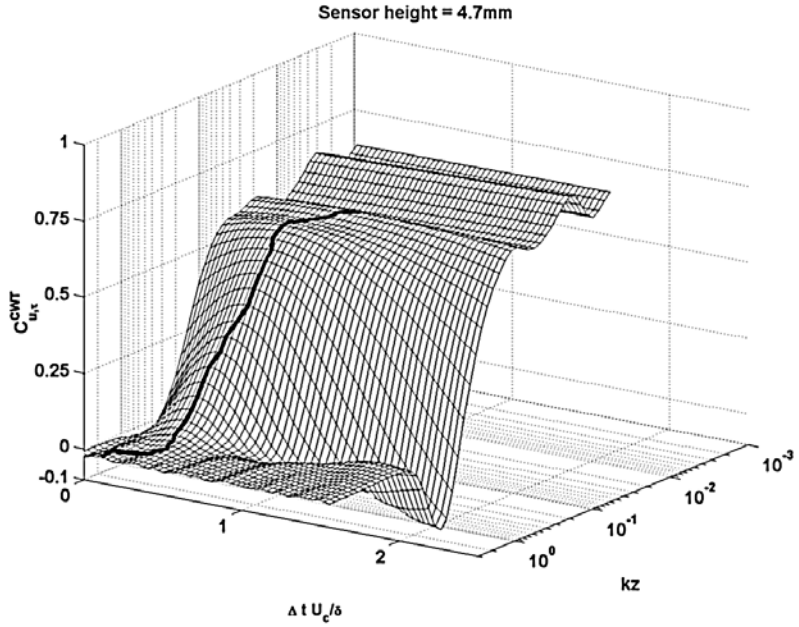

Figure 6. Correlation between horizontal velocity (u) and shear stress (τ) computed in the wavelet domain, as explained in the text, for z = 4.7 mm. The bold solid line shows the ''migration'' of the time lag at which the maximum correlation at each scale is obtained.

size equal to or slightly larger than the grid size). This formulation guarantees that the mean shear stress is preserved. The mean shear stress $\langle\tau\rangle$ is computed from the average velocity $\langle\tilde{u}\rangle$ using similarity theory (e.g., the well-known law of the wall in the case of zero buoyancy).

[25] 2. Another formulation results from the direct application of similarity theory to compute τ as a function of $\tilde{u}$ [e.g., *Moeng*, 1984; *Albertson and Parlange*, 1999]. Even though this formulation does not guarantee that the average shear stress is preserved, it is easier to use than equation (6) when the mean velocity $\langle\tilde{u}\rangle$ is difficult to estimate (e.g., boundary layers over heterogeneous surfaces).

[26] In the discussion that follows, we focus on the formulation given by equation (6). Note that equation (6) implies that the two-point linear correlation between surface shear stress and horizontal velocity is 1 at all resolved scales (larger than the filter size). However, our results indicate that this is not the case. In fact, equation (5) provides a quantification of how the correlation between u and τ changes with scale. Moreover, our results suggest that the filter size and its relative magnitude compared to the height of the first grid point in a simulation (which depends on the grid size and aspect ratio) is expected to affect the performance of the surface boundary condition.

[27] Of particular interest from a modeling/parameterization perspective is the significance of the plateau in the MC curves for scales larger than the boundary layer height, δ. As one looks at the interaction of two processes at larger and larger scales (i.e., smoothing), intuitively, one would expect a monotonic increase in correlation. However, the plateau suggests otherwise. The practical implication of this is that a linear parameterization of τ in terms of u (as is often done in high-resolution numerical models for the surface boundary condition) cannot explain the dependence between these two variables beyond the linear correlation suggested by the plateau value (which is a function of z/δ) of Figure 7.

[28] It is important to note that there is a fundamental difference between the wavelet analysis filtering and the filtering operation performed when the boundary condition (equation (6)) is implemented. While in the former, only the features corresponding to the scale of the analyzing function are extracted from the signal; in the latter, all features larger than the size of the filter are retained. Consequently, one must remember that the correlation that one obtains from wavelet analysis gives explicitly the contribution of each scale, while a filtering operation would give a correlation that is a combination of correlations corresponding to scales larger than the filter size. To examine how the plateau value of the MC obtained via wavelet analysis compares to that obtained by box filtering, the velocity and shear stress signals were filtered using a box function (i.e., a moving average). Several lengths (widths) of the box function were chosen for the filtering operation. Figure 8 shows, for z = 4.7 mm, the wavelet maximum correlation as well as the maximum correlation obtained from the filtering procedure described earlier. In the inertial subrange the maximum correlation from filtering (stars) does not change with increasing scale. For $kz \lesssim 1$, there is an increase in correlation, and finally, beyond the boundary layer height, the correlation reaches a plateau. The value of the plateau for the filtered signals matches that obtained by the wavelet analysis (in this case, $-1/2\log(4.7/64) \approx 0.58$ from equation (5)). This was expected since, as said before, the correlation of the filtered quantities is a combination of correlation contributions (from each scale larger than the filter length), which for scales larger than δ are approximately the same.

[29] Of particular importance is the value of this plateau. Since δ is constant for any given boundary layer, our analysis suggests that the value of the plateau increases with decreasing height (see Figure 7). Furthermore, the plateau is expected to reach a value of 1 for $z/\delta \approx 10^{-2}$

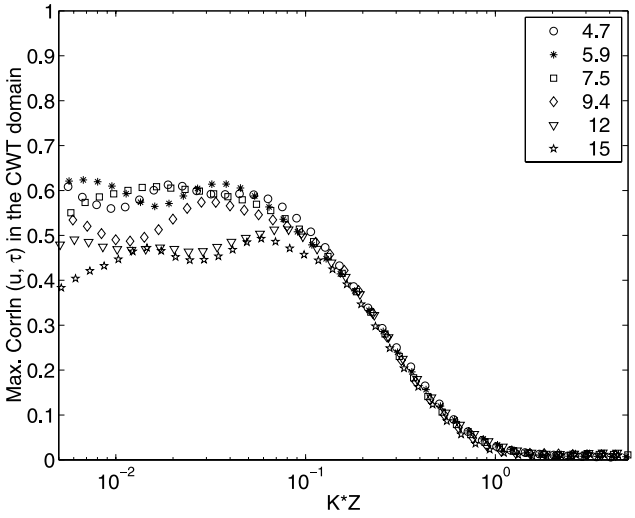

Figure 7. Plot of maximum correlation (of the surfaces shown in Figure 6) at each scale versus *kz* for different sensor heights. The shape of the curves suggests three distinct regions of contribution to the overall correlation: the inertial subrange(−5/3 spectral slope), where the contribution of correlation is virtually negligible; the production subrange (−1 spectral slope), where the correlation increases as a log law with a slope of −1/2; and the range in which scales are larger than the boundary layer height, where there is no increase in correlation. The collapse of the curves indicates a possible universality in the dependence of correlation on scale.

(see equation (5)). In wall units, this is equivalent to a height of $z^+ = 14$, which falls inside the buffer layer ($5 < z^+ < 30$) that corresponds to the transition between the log layer and the viscous sublayer below [see, e.g., *Tennekes and Lumley*, 1994]. This limiting behavior of the correlation can be understood considering that throughout the viscous sublayer ($0 < z^+ < 5$) the shear stress is dominated by viscosity, and turbulent (Reynolds) shear stress is negligible. This explains why the boundary condition is not an issue in simulations of low-Reynolds-number and moderate-Reynolds-number boundary layers, where the grid size is smaller than the depth of the viscous sublayer. On the other hand, in high-Reynolds-number boundary layers (e.g., the ABL), computational limitations impose the location of the first grid point well into the log layer. This affects the maximum correlation between surface shear stress and velocity (equation (5) and Figure 7) and, consequently, the reliability of the surface boundary condition (equation (6)).

6. Conclusions and Future Work

[30] High-frequency measurements obtained in a wind tunnel experiment were used to quantify the multiscale interactions between surface shear stress and wind velocity in a turbulent boundary layer. In particular, with the aid of wavelet analysis we were able to quantify the degree of correlation between the two variables as a function of scale. This information is essential in understanding the performance of surface boundary condition parameterizations, typically used in large-eddy simulations, that compute the "instantaneous" shear stress as a linear function of the velocity at the first grid point at the grid/filter scale.

[31] Our results suggest the presence of three distinct ranges of scales of interaction, corresponding to three well-known ranges in turbulent boundary layers. For the range of scales corresponding to the inertial subrange of turbulence the contribution to the overall correlation between shear stress and velocity is negligible. In the range of scales beyond the boundary layer height the correlation contribution is significant but constant. This, possibly, points to the maximum correlation that one can achieve via a simple linear parameterization relating velocity and shear stress for the surface boundary condition. Finally, in the energy production subrange the correlation contribution follows a log law with a slope of −1/2. We hypothesize that this log law behavior is universal, given the fact that correlation curves are identical for any height under appropriate normalization. On the other hand, we speculate that the slope of the log law is dependent on the flow conditions. From a modeling/parameterization point of view the universal behavior of the interaction between shear stress and velocity can help one understand and predict the performance and limitations of surface boundary condition parameterizations as a function of grid scale, height of the first grid point, and grid aspect ratio. In large-eddy simulations the grid scale typically falls inside the energy production range.

[32] Future work will explore the effect of high Reynolds number on our results (i.e., universality, slope of the log law), using data collected in the ABL. This type of data will also allow us to study the effect of atmospheric stability on the multiscale interactions between shear stress and velocity and its implications for boundary condition parameterizations. It is noted that field measurements of surface shear stress require the development of new surface shear sensors, with a high enough frequency response to provide information at all relevant scales. Until this technology is further developed, wind tunnel data offer the only means to study

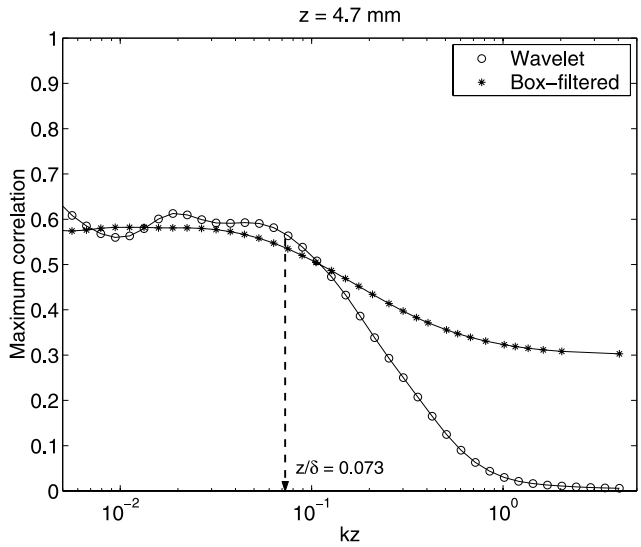

Figure 8. Maximum correlation obtained by wavelet analysis (circles) and filtering (stars) for $z = 4.7$ mm. See text for a detailed explanation.

these interactions for the purpose of improving numerical model parameterizations.

[33] **Acknowledgments.** The work presented here has been partially supported by research grants to the principle investigators (NSF (ATM-013094) and NASA (NAG 5-7715) to Foufoula-Georgiou; NSF (EAR-0094200) and NASA (NAG5-10569 and NAG5-11801) to Porté-Agel; and NSF (EAR-0120914) as part of the National Center for Earth-Surface Dynamics (NCED) at the University of Minnesota). The first author would like to thank Minnesota Supercomputing Institute for their computing and financial support. Many thanks to Ivan Marusic and Gary Kunkel for kindly providing us with the shear stress and velocity measurements. We thank the reviewers, whose insightful comments helped improve the clarity of the presentation.

References

Albertson, J. D., and M. B. Parlange, Surface length scales and shear stress: Implications for land-atmosphere interaction over complex terrain, *Water Resour. Res.*, *35*, 2121–2132, 1999.

Arnéodo, A., E. Bacry, S. Manneville, and J. F. Muzy, Analysis of random cascades using space-scale correlation functions, *Phys. Rev. Lett.*, *80*, 708–711, 1998.

Brunet, Y., and S. Collineau, Wavelet analysis of diurnal and nocturnal turbulence above a maize crop, in *Wavelets in Geophysics*, edited by E. Foufoula-Georgiou and P. Kumar, pp. 129–150, Academic, San Diego, Calif., 1994.

Chew, Y. T., B. C. Khoo, C. P. Lim, and C. J. Teo, Dynamic response of hot-wire-anemometer. part II: A flush-mounted hot-wire and hot-film probes for wall shear stress measurements, *Meas. Sci. Technol.*, *9*(5), 764–778, 1998.

Daubechies, I., *Ten Lectures on Wavelets*, Soc. Ind. Appl. Math., Philadelphia, Pa., 1992.

Farge, M., Wavelet transforms and their applications in turbulence, *Ann. Rev. Fluid Mech.*, *24*, 395–457, 1992.

Hagelberg, C. R., and N. K. Gamage, Applications of structure preserving wavelet decompositions to intermittent turbulence: A case study, in *Wavelets in Geophysics*, edited by E. Foufoula-Georgiou and P. Kumar, pp. 45–80, Academic, San Diego, Calif., 1994.

Howell, J. F., and L. Mahrt, An adaptive decomposition: Applications to turbulence, in *Wavelets in Geophysics*, E. Foufoula-Georgiou and P. Kumar, pp. 107–128, Academic, San Diego, Calif., 1994.

Katul, G., and C.-R. Chu, A theoretical and experimental investigation of energy-containing scales in the dynamic sublayer of boundary-layer flows, *Boundary Layer Meteorol.*, *86*, 279–312, 1998.

Katul, G., M. B. Parlange, and C.-R. Chu, Intermittency, local isotropy and non-Gaussian statistics in atmospheric surface layer turbulence, *Phys. Fluids A*, *6*(7), 2480–2492, 1994.

Mallat, S., A theory for multiresolution signal decomposition: The wavelet representation, *IEEE Trans. Pattern Anal. Mach. Intel.*, *11*, 674–693, 1989a.

Mallat, S., Multifrequency channel decomposition of images and wavelet models, *IEEE Trans. Acoust. Speech Signal Process.*, *37*, 2091–2110, 1989b.

Marusic, I., G. J. Kunkel, and F. Porté-Agel, Experimental study of wall boundary conditions for large-eddy simulation, *J. Fluid Mech.*, *446*, 309–320, 2001.

Meneveau, C., Analysis of turbulence in the orthonormal wavelet representation, *J. Fluid Mech.*, *232*, 469–520, 1991.

Meneveau, C., and T. S. Lund, On the Lagrangian nature of the turbulence energy cascade, *Phys. Fluids A*, *6*(8), 2820–2825, 1994.

Moeng, C.-H., A large-eddy simulation for the study of planetary boundary-layer turbulence, *J. Atmos. Sci.*, *41*(13), 2052–2062, 1984.

Perry, A. E., S. Henbest, and M. S. Chong, A theoretical and experimental study of wall turbulence, *J. Fluid Mech.*, *165*, 163–199, 1986.

Piomelli, U., and E. Balaras, Wall-layer models for large-eddy simulations, *Ann. Rev. Fluid Mech.*, *34*, 349–374, 2002.

Piomelli, U., J. Ferziger, and P. Moin, New approximate boundary conditions for large eddy simulations of wall-bounded flows, *Phys. Fluids A*, *1*(6), 1061–1068, 1989.

Porté-Agel, F., C. Meneveau, and M. B. Parlange, A scale-dependent dynamic model for large-eddy simulation: Application to a neutral atmospheric boundary layer, *J. Fluid Mech.*, *415*, 261–284, 2000.

Roy, S. B., and R. Avissar, Scales of response of the convective boundary layer to land-surface heterogeneity, *Geophys. Res. Lett.*, *27*(4), 533–536, 2000.

Schumann, U., Subgrid scale model for finite difference simulations of turbulent flows in plane channels and annuli, *J. Comput. Phys.*, *18*, 376–404, 1975.

Tennekes, H., and J. L. Lumley, *A First Course in Turbulence*, MIT Press, Cambridge, Mass., 1994.

M. Carper, E. Foufoula-Georgiou, F. Porté-Agel, and V. Venugopal, St. Anthony Falls Laboratory, University of Minnesota, Mississippi River at 3rd Avenue SE, Minneapolis, MN 55414, USA. (carper@msi.umn.edu; efi@umn.edu; fporte@umn.edu; venu@msi.umn.edu)